






Emergence of bond-dependent highly anisotropic magnetic interactions in Sr_4RhO_6 : A theoretical study

Shishir Kumar Pandey ^{1,2,*}, Qiangqiang Gu ^{2,3}, Yihao Lin ¹, Rajarshi Tiwari ⁴, and Ji Feng ^{1,5}

¹International Center for Quantum Materials, School of Physics, Peking University, Beijing 100871, China

²AI for Science Institute, Beijing, China

³School of Mathematical Science, Peking University, Beijing 100871, China

⁴School of Physics, AMBER and CRANN Institute, Trinity College Dublin, Dublin 2, Ireland

⁵Hefei National Laboratory, Hefei 230088, China



(Received 30 September 2022; revised 25 November 2022; accepted 13 February 2023; published 9 March 2023)

The quantum spin liquid as a natural ground state of the Kitaev model has led to a quest for new materials candidates hosting Kitaev physics. Yet, there are very few material candidates in this category. Using a combination of *ab initio* and model Hamiltonian methods, we propose that the Ruddlesden-Popper compound Sr_4RhO_6 belongs to this category. With a tight-binding model and exact-diagonalization approach, we show that despite substantial trigonal-like distortion, the electronic and magnetic properties of Sr_4RhO_6 can be well described in terms of pseudospin-1/2 states. Magnetic interactions among pseudospins, estimated using the second-order perturbation method, are highly bond-dependent anisotropic in nature with two particularly noticeable features, antiferromagnetic Kitaev and Dzyaloshinskii-Moriya interactions. The gapped spin-wave spectrum of Sr_4RhO_6 obtained with linear spin-wave theory is consistent with the underlying magnetic frustration. Additional analysis of the role of individual or a particular combination of magnetic interactions reveals that the spin-wave spectrum of Sr_4RhO_6 is a combined effect of the highly anisotropic interactions, and a relatively simpler minimal model may not be plausible in the current case. The crucial insights about coupling between the local structural features and magnetic properties of Sr_4RhO_6 obtained in this study may be helpful for future studies belonging to this class.

DOI: [10.1103/PhysRevB.107.115119](https://doi.org/10.1103/PhysRevB.107.115119)

I. INTRODUCTION

The orbital and spin angular momentum of an electron are coupled through a relativistic effect called spin-orbit coupling (SOC). Many interesting phenomena, such as the anomalous Hall effect, manipulation of spin currents, and the emergence of topological properties in weakly correlated systems, have been extensively studied [1–3]. However, strongly correlated materials host even richer physics because of the presence of additional interactions such as crystal field splitting (Δ^{CF}) and on-site Hubbard interaction (U), often competing with SOC [4,5]. This competition gives rise to exotic phenomena such as the realization of unconventional superconductivity [6–8], emergence of topological phases [9], and Kitaev physics [10]. Among these examples, Kitaev physics [11] in particular has recently received a lot of attention as a driving mechanism in the realization of quantum spin liquid states [12,13].

The work of Jackeli and Khaliullin [10] accelerated the progress towards the realization of Kitaev physics in real materials. Their proposal was based on magnetic interactions between pseudospins on a honeycomb lattice of transition-metal ions originating from the interplay of a strong electrostatic crystal field (CF) of anions and SOC at transition-metal sites. The five degenerate d orbitals of a transition-metal atom split into triply degenerate t_{2g} and doubly degenerate

e_g orbitals due to Δ^{CF} [see Fig. 1(a)]. The energetically lower t_{2g} manifold further splits in the presence of SOC to form the half-filled pseudospin $J_{\text{eff}} = \frac{1}{2}$ states dominating the low-energy space of materials. Magnetic interactions between these $J_{\text{eff}} = \frac{1}{2}$ pseudospin states was proposed to be dominantly Kitaev type. Cobaltates [14–23], iridates [24–31], and $\alpha\text{-RuCl}_3$ [32–36] are some of the examples falling in this category. Recent studies on Ir-based double perovskite compounds have further widened the horizon of Kitaev physics on a frustrated face-centered cubic lattice formed by magnetic ions with a spatially separated octahedral environment [37–41].

These pseudospin $J_{\text{eff}} = \frac{1}{2}$ doublets are Kramers's doublet, which relate to each other by time-reversal symmetry and are degenerate when time-reversal symmetry is preserved. The associated operators, J_{eff}^μ , where $\mu = x, y, z$, thus follow the spin commutation relations. Only in the limits $\Delta^{\text{CF}} \rightarrow \infty$ and when the splitting among the t_{2g} manifold due to additional trigonal (tetragonal) distortions $\Delta_{\text{tri}}^{\text{CF}} (\Delta_{\text{tet}}^{\text{CF}}) \rightarrow 0$, can a pure $J_{\text{eff}} = \frac{1}{2}$ state be realized.

However, the real materials mentioned above are far from these ideal limits, making the situation even more complex. Such complexities are inevitable when a minor change in the details of these interactions may have dramatic effects on the macroscopic behavior of the material. For example, in iridates, despite the presence of additional $\Delta_{\text{tri}}^{\text{CF}} (\Delta_{\text{tet}}^{\text{CF}})$ distortions which are responsible for mixing between $J_{\text{eff}} = \frac{1}{2}$ and $\frac{3}{2}$

*shishir.kr.pandey@gmail.com

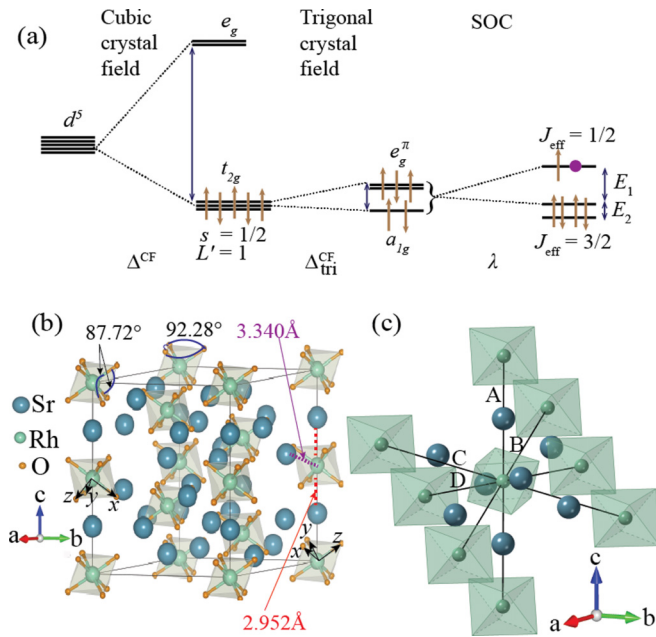


FIG. 1. (a) J_{eff} picture for a d^5 system arising from the octahedral crystal field (Δ^{CF}) and spin-orbit coupling (λ). Additional splitting of the t_{2g} states into a singlet a_{1g} and a doublet e_g^{π} due to trigonal-like distortions ($\Delta_{\text{tri}}^{\text{CF}}$). SOC further leads to a $J_{\text{eff}}=1/2$ doublet and two $J_{\text{eff}}=3/2$ doublets separated by E_2 . E_1 is the energy separation between $J_{\text{eff}}=1/2$ and the closest $J_{\text{eff}}=3/2$ doublet. (b) Side view of the Sr_4RhO_6 crystal structure. Spatially separated octahedron are evident. Local x , y , and z axes on two of the octahedron are shown. a , b , and c are the global crystallographic axes. Two kinds of color-coded Rh-Sr bonds along with O-Rh-O bond angles obtained after optimization of the crystal structure are shown. (c) Extended local environment (including Sr atoms) around an Rh atom in Sr_4RhO_6 . Four types of Rh-Rh nearest neighbors A, B, C, and D bonds, with Rh-O octahedra on these bonds, are also shown.

states [27,31], the large SOC of Ir $5d$ orbitals still allows a $J_{\text{eff}} = \frac{1}{2}$ description of the magnetic properties. However, the same cannot be assumed for a $4d$ transition-metal compound where the SOC strength is nearly half of its $5d$ counterpart and $\Delta_{\text{tri}}^{\text{CF}}$ ($\Delta_{\text{tet}}^{\text{CF}}$) distortions of octahedra might be comparable to the SOC strength. This inhibits any generic rule for behavior prediction of such materials and, hence, a case-to-case study is often required.

The scarcity of $4d$ magnetic compounds with $J_{\text{eff}} = \frac{1}{2}$ behavior makes it even more difficult to obtain any comprehensive understanding. To the best of our knowledge, the only example of magnetic material in this category is $\alpha\text{-RuCl}_3$ which has been the subject of extensive theoretical and experimental investigations [32–36]. Other $4d$ materials, such as Li_2RhO_3 , Sr_2RhO_4 , and some theoretically predicted Rh- and Ir-based fluorides, are either nonmagnetic (Li_2RhO_3 shows spin-glass behavior) or paramagnetic in nature [42–44]. In the quest for new Kitaev candidates, Sr_4RhO_6 is another possible example of a $4d$ oxide [45,46]. Materials such as Sr_4RhO_6 and some Ir-based double perovskites [37–41] with isolated metal-anion octahedra [as shown in Fig. 1(b)] may possess an advantage over materials with edge-shared geometry because the larger spatial separation between the magnetic ions in

the former can minimize the direct overlap of d orbitals as compared to edge-shared geometry. This in turn may result in suppression of additional *undesirable* nearest-neighbor as well as farther-neighbor Heisenberg-like isotropic coupling. Sr_4RhO_6 is believed to exhibit an ideal cubic octahedral environment on Rh sites [46] in a centrosymmetric crystal structure. Such a distinctive feature may lead to the realization of *pure* $J_{\text{eff}} = 1/2$ states, a feature not realized in any of the previously mentioned Kitaev candidate materials. Despite purportedly having such lucrative features with the possibility of hosting rich physics, it is surprising to find no theoretical study dedicated to this material and hence is the focus of our study in this article.

In this study, using a combination of first-principles calculations and a tight-binding (TB) model, we first show that contrary to the earlier belief [46], the Rh- O_6 octahedra in Sr_4RhO_6 is not perfect and the octahedral crystal field at Rh sites has additional trigonal-like distortions originating from the influence of the extended environment of Sr atoms. Using the exact-diagonalization (ED) technique, we show that despite such a distortion, mixing between $J_{\text{eff}} = 1/2$ – $3/2$ states is small and a description of low-energy space in terms of $J_{\text{eff}} = 1/2$ states is still valid in this material. Magnetic interaction among these pseudospins estimated using second-order perturbation theory shows highly bond-dependent anisotropic behavior with additional diagonal/off-diagonal terms appearing alongside two particularly noticeable features, antiferromagnetic (AFM) Kitaev and Dzyaloshinskii-Moriya interactions (DMIs) on some of the first-nearest-neighbor (1NN) Rh-Rh bonds. We attribute the appearance of DMIs to the local inversion symmetry breaking due to the extended environment of Sr^{+2} ions. The second- and third-nearest-neighbor interactions are found to be negligibly small. The classically optimized magnetic ground state brings an AFM configuration which is energetically close to the previously proposed magnetic structure. Spin-wave spectrum calculated using linear spin-wave theory is found to be gapped throughout the Brillouin zone, consistent with the underlying frustrated magnetic interactions. The origin of various features of the spectrum is analyzed separately by examining the role of different magnetic interaction terms in the spin Hamiltonian. This analysis establishes the fact that the spectrum is a combined effort of all these highly anisotropic magnetic interactions, and a relatively simpler minimal magnetic model may not be plausible in the current case. Our study provides crucial insights for compounds belonging to this class.

II. METHODS

A. *Ab initio* calculations

Density functional theory (DFT) calculations have been performed using the projector-augmented wave method [47,48], implemented within the Vienna *ab initio* simulation package (VASP) [49]. The Perdew-Burke-Ernzerhof functional [50] is used for the exchange-correlation functional within the generalized gradient approximation (GGA) formalism. We start with the experimental lattice parameters of a trigonal crystal system of Sr_4RhO_6 with centrosymmetric space group

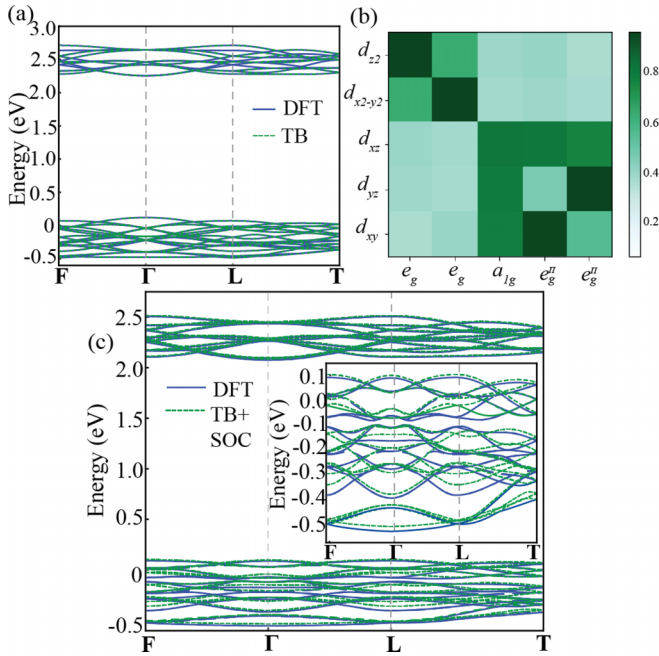


FIG. 2. (a) Band structure plot from the *ab initio* and Wannier-based TB model calculations considering all the Rh *d* orbitals in the basis. (b) Graphical representation of eigenvectors of the matrix in Eq. (1). In columnwise representation of eigenvectors, each row represents the absolute weight of the individual orbitals. Labeling of eigenstates is done in accordance with Fig. 1(a). (c) Fitting of *ab initio* SOC band structure with Wannier-based tight-binding model after including the on-site SOC term in the Hamiltonian. The inset shows the fitting near the Fermi level, which is set to zero in all the plots.

$R\bar{3}c$ (No. 167), which are $|\mathbf{a}| = |\mathbf{b}| = 9.740 \text{ \AA}$, $|\mathbf{c}| = 11.840 \text{ \AA}$; $\alpha = \beta = 90^\circ$ and $\gamma = 120^\circ$ [46]. Using plane-wave cutoff energy 550 eV, $4 \times 4 \times 2$ Γ -centered k mesh, and energy convergence criteria of 10^{-5} eV, we optimize the lattice parameters with the experimentally proposed magnetic ground state (accommodated within 24 Rh atoms in a $2 \times 2 \times 1$ supercell) considering the SOC effect at the self-consistent level. A DFT+ U approach employing the Liechtenstein [51] scheme with on-site Coulomb interaction $U = 2.5$ eV and exchange interaction $J_H = 0.9$ eV was used. The values of the U and J_H parameters are consistent with the previous study [46]. Optimized a and b lattice constants were found to be overestimated by $\sim 3.1\%$, while c remains the same. Since this change in lattice constants is significant, we have used the optimized structure in further calculations.

B. Estimation of electronic parameters

The non-spin-polarized TB Hamiltonian (H_{TB}) in the local axes framework [see Fig. 1(b)] was calculated by projecting onto all five Rh-*d* orbitals using the Wannierization procedure [52] and is shown in Fig. 2(a). On the two symmetry inequivalent Rh sites, the octahedron is rotated around the C_3 axis, which is along the crystallographic c axis. We choose the local axes (x, y, z) along oxygen atoms on one of the Rh sites obeying $c = x + y + z$ and rotate these axes on the other Rh site by a unitary transformation to obtain the identical form of

the CF matrix on the two sites. The crystal field matrix on a site i (Δ_i^{CF}) is extracted from the on-site part of H_{TB} , which obeys the crystal's C_3 symmetry. To extract the SOC strength (λ), we fit the *ab initio* band structure, where the SOC was included at the self-consistent level, with H_{TB} after adding the on-site $H_{soc} = \sum_i \lambda \mathbf{L}_i \cdot \mathbf{s}_i$ term [53]. The fitting is shown in Fig. 2(c), with the inset showing the fitting near the Fermi level. It brings $\lambda = 90$ meV. This value is smaller than the considered value for isoelectronic α - RuCl_3 ($\lambda = 140$ meV) [36,54] and a recently estimated value of 175 meV for the Rh atom [55]. However, on a later stage, we will show that considering these three values does not bring any qualitative changes in the magnetic interactions and, hence, for the rest of the discussion in the manuscript, we choose $\lambda = 140$ meV. We estimate the Coulomb matrix elements $U_{ijkl}(\omega = 0)$ within the constrained random phase approximation (cRPA). To this end, we neglect the screening effects for all five Rh *d* orbital states which are energetically well separated from other states [56–58]. The estimated parameters are $U = 2.474$ eV and $J_H = 0.106$ eV, which were further used in our multiband Hubbard model.

III. RESULTS

A. Structural analysis and electronic properties

Under a large Δ_i^{CF} , the low-energy space Rh- $4d^5$ ions can be described by a single hole within the t_{2g} manifold with effective spin moment $s = 1/2$ and effective orbital angular momentum $L' = 1$. The spin-orbit coupling then leads to an effective total angular momentum of $\mathbf{J}_{\text{eff}} = \mathbf{s} - \mathbf{L}'$, resulting in doubly degenerate pseudospin-1/2 states forming low-energy space in this material. This is schematically shown in Fig. 1(a). However, the lowering of cubic O_h symmetry of the octahedron due to the additional Δ_{tet}^{CF} (Δ_{tet}^{CF}) terms can invalidate this picture. Hence it is important to first examine whether the Rh- O_6 octahedra in Sr_4RhO_6 retains the O_h symmetry, as was proposed earlier in Ref. [46].

In this experimental crystal structure, all six Rh-O bond lengths are $\sim 2.044 \text{ \AA}$, while O-Rh-O bond angles are quite close to the ideal 90° , with the largest deviation being 0.1° . However, full structural optimization with the magnetic ground state in our DFT calculation brings substantial changes in the a and b lattice constants, along with the changes in the local octahedral environment. The optimization enhanced a and b lattice constants to 10.046 \AA and also all six Rh-O bond lengths elongated to 2.109 \AA . The structural optimization also alters the O-Rh-O bond angles to 92.28 and 87.72° [see Fig. 1(b)]. Also, out of eight Sr neighbors in the extended environment of Rh atoms, two ‘‘apical’’ Sr atoms along the c axis are at 2.952 \AA distance, while the other six nonapical Sr are at 3.340 \AA in the optimized structure. This is shown in Fig. 1(b) (short Rh-Sr distances are along A bonds and long ones are along B/C/D bonds). These two kinds of Rh-Sr distances were 2.960 and 3.238 \AA in the starting structure. Almost similar Rh-Rh 1NN distances $\sim 5.98/6.0 \text{ \AA}$ of all eight bonds before optimization have now changed substantially to ~ 5.9 and 6.13 \AA for two A bonds and six B/C/D bonds, respectively. Thus, optimization of structure results in substantial changes in Rh-O, nonapical Rh-Sr, and overall Rh-Rh

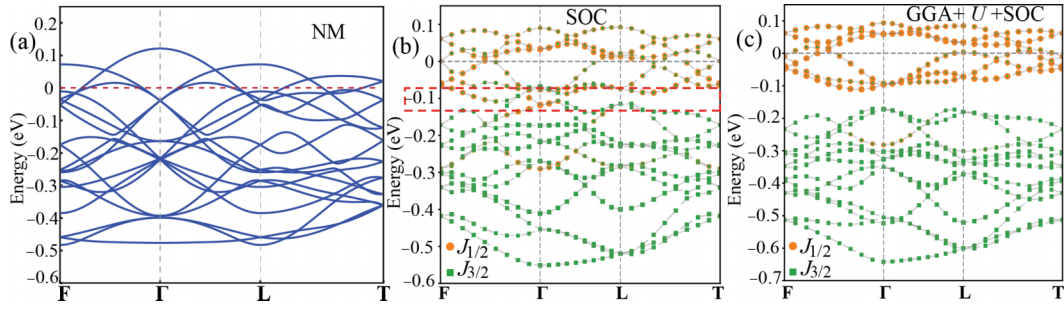


FIG. 3. *Ab initio* band structure plots near the Fermi level. Case of (a) nonmagnetic (NM), (b) SOC included, and (c) SOC + U (on Rh d orbitals) band structure projected onto J_{eff} states. Fermi level is set to 0 eV. The red dashed box in (b) shows the energy window where the separation of the $J_{\text{eff}}=1/2$ bands from other $J_{\text{eff}}=3/2$ bands take place with inclusion of SOC. A clear $J_{\text{eff}}=1/2$ character is apparent at the Fermi level in (c).

bond lengths, and is consistent with enhancement of the a and b lattice constants.

In order to understand how these changes in crystal structure affect the CF, we set up a TB model with a d orbital basis of $\psi^\dagger = [d_{z^2}^\dagger, d_{x^2-y^2}^\dagger, d_{xz}^\dagger, d_{yz}^\dagger, d_{xy}^\dagger]$ using the Wannierization procedure as mentioned in Sec. II [fitting is shown in

Fig. 2(a)]. The CF matrix Δ_i^{CF} obtained from H_{TB} is given in Eq. (1). Entries in the matrix are in units of eV. One can clearly see that this CF matrix obeys the C_3 symmetry restriction as the off-diagonal elements within the t_{2g} manifold have nearly the same absolute values within an error bar of 5 meV.

$$\Delta_i^{\text{CF}} = \begin{bmatrix} 2.5379 & -0.0006 & -0.1292 & 0.0987 & -0.0517 \\ -0.0006 & 2.5474 & 0.0150 & -0.0088 & -0.0762 \\ -0.1292 & 0.0150 & 0.1127 & 0.0499 & 0.0531 \\ 0.0987 & -0.0088 & 0.0499 & 0.1055 & -0.0547 \\ -0.0517 & -0.0762 & 0.0531 & -0.0547 & 0.1138 \end{bmatrix} \quad (1)$$

By diagonalizing this matrix, one can find that the $t_{2g}-e_g$ crystal field splitting ($\Delta_i^{t_{2g}-e_g}$) is ~ 2.630 eV, while the triply degenerate t_{2g} splits into a a_{1g} singlet and e_g^π doublet by $\Delta_{\text{tri}}^{\text{CF}} \sim 160$ meV, with the doublet being higher in energy than the singlet. The corresponding eigenvectors are graphically represented in Fig. 2(b), where each column in the 5×5 graph represents an eigenvector and with the row representing the absolute weight of individual orbitals. This representation clearly highlights the nature of Δ_i^{CF} in Sr_4RhO_6 , which has been depicted in Fig. 1(a).

This particular form of Δ_i^{CF} can be understood as follows. The shorter ‘‘apical’’ Sr-Rh bond passes through the center of two triangular faces of Rh-O₆ octahedra, as shown in Figs. 1(b) and 1(c). This bond is also one of the four threefold rotational symmetry (C_3) axes of the Rh-O₆ octahedra. The electrostatic repulsion along these shorter bonds behaves as compressing strain, causing changes in the Rh-O bond lengths and O-Rh-O bond angles. This is analogous to the case of trigonal distortions, where bond distortions take place along one of the four C_3 axes of the octahedra. Thus, in Sr_4RhO_6 , an extended anisotropic environment of Sr atoms produces a nonspherical crystalline potential responsible for the additional $\Delta_{\text{tri}}^{\text{CF}}$ of the Rh-O₆ octahedra. The cubic O_h symmetry then lowers to $C_{3i} (-3)$ in this case.

Distortions such as $\Delta_{\text{tri}}^{\text{CF}}$ tend to lower the energy separation between the $J_{\text{eff}}=1/2$ and $3/2$ states. This causes a genuine concern about the effect of SOC on the electronic structure of Sr_4RhO_6 and whether the strength of SOC in Sr_4RhO_6 is

sufficient enough to separate out these two states. To examine this point, we calculated the *ab initio* band structures for three cases: (i) nonmagnetic, (ii) with SOC, and (iii) with SOC + U . SOC was included at the self-consistent level in these calculations.

In Fig. 3, we only show the bands near the Fermi level which are dominantly contributed by t_{2g} orbitals. We projected the band structures onto J_{eff} states with the form given below,

$$\begin{aligned} \left| \frac{1}{2}, \pm \frac{1}{2} \right\rangle &= \frac{1}{\sqrt{3}} \left(\mp \left| d_{xy}, \pm \frac{1}{2} \right\rangle \mp i \left| d_{xz}, \mp \frac{1}{2} \right\rangle - \left| d_{yz}, \mp \frac{1}{2} \right\rangle \right), \\ \left| \frac{3}{2}, \pm \frac{3}{2} \right\rangle &= \frac{1}{\sqrt{2}} \left(-i \left| d_{xz}, \pm \frac{1}{2} \right\rangle \mp \left| d_{yz}, \pm \frac{1}{2} \right\rangle \right), \\ \left| \frac{3}{2}, \pm \frac{1}{2} \right\rangle &= \frac{1}{\sqrt{6}} \left(2 \left| d_{xy}, \pm \frac{1}{2} \right\rangle - i \left| d_{xz}, \mp \frac{1}{2} \right\rangle \mp \left| d_{yz}, \mp \frac{1}{2} \right\rangle \right). \end{aligned}$$

There are two main points to be noticed in Fig. 3. First, that inclusion of SOC substantially changes the band structure. This is apparent from comparing the non-spin-polarized band structure plot in Fig. 3(a) and the SOC-included band structure plot shown in Fig. 3(b). In particular, SOC leads to separation of the $J_{\text{eff}}=1/2$ bands near -0.1 eV [red box in Fig. 3(b)] from the other bands ($J_{\text{eff}}=3/2$ bands) near -0.1 eV. Inclusion of U on Rh d states further contributes to this band separation, as shown in Fig. 3(c), and the dominant contribution near the Fermi level is now clearly shown to have $J_{\text{eff}}=1/2$ character. Imposition of the magnetic ground state in the band structure calculation (not shown) fully opens the

gap at the Fermi level, making it insulating. This is similar to the case of α -RuCl₃ [35]. From this analysis of the electronic structure, one can conclude that the electronic structure of Sr₄RhO₆ is the combined efforts of U , SOC, and magnetism. Having examined the role of SOC, one can further quantify the $J_{\text{eff}}=1/2$ and $3/2$ states' admixture due to $\Delta_{\text{tri}}^{\text{CF}}$ by considering a multiband Hubbard model for an isolated Rh⁺⁴ ion. This is discussed in the next section.

B. On-site Hamiltonian and the atomic features

One way to estimate the extent of mixing between the $J_{\text{eff}}=1/2$ and $3/2$ states is by calculating the projection of "pure" $J_{\text{eff}}=1/2$ and $3/2$ states for the case when $\Delta_{\text{tri}}^{\text{CF}} = 0$ onto the "true" $J_{\text{eff}}=1/2$ obtained with Eq. (1). These states are atomic features and hence can be described in an isolated atom limit. In this limit, a multiband Hubbard Hamiltonian at site i in the five-orbital basis is

$$\begin{aligned}
 H_0 &= H_{\text{cf}} + H_{\text{soc}} + H_{\text{int}} \\
 &= \sum_{i,\sigma} \psi_{i\sigma}^\dagger \Delta_i^{\text{CF}} \psi_{i\sigma} + \sum_i \lambda \mathbf{L}_i \cdot \mathbf{s}_i \\
 &\quad + \frac{U}{2} \sum_{i,\alpha} n_{i\alpha\sigma} n_{i\alpha\sigma'} + \frac{U'}{2} \sum_{i,\alpha \neq \beta} n_{i\alpha} n_{i\beta} \\
 &\quad - \frac{J_{\text{H}}}{2} \sum_{i,\sigma,\sigma',\alpha \neq \beta} \psi_{i\alpha\sigma}^\dagger \psi_{i\alpha\sigma'} \psi_{i\beta\sigma'}^\dagger \psi_{i\beta\sigma} \\
 &\quad - \frac{J'}{2} \sum_{i,\sigma \neq \sigma',\alpha \neq \beta} \psi_{i\alpha\sigma}^\dagger \psi_{i\beta\sigma'} \psi_{i\alpha\sigma'}^\dagger \psi_{i\beta\sigma}. \quad (2)
 \end{aligned}$$

In the above expression, U/U' are intraorbital/interorbital Hartree energies; and J_{H} and J' are the Hund's coupling and pair hopping interaction, respectively. Rotational invariance in the isolated atom limit dictates the relationships $U' = U - 2J_{\text{H}}$ and $J_{\text{H}} = J'$. We use $U = 2.474$ eV and $J_{\text{H}} = 0.106$ eV, which are estimated from cRPA as mentioned in Sec. II, and $\lambda = 140$ meV is considered. We diagonalize the above Hamiltonian considering five electrons of Rh⁺⁴ ions which give a total of 252 eigenstates, the lowest two and the next four of which are the $J_{\text{eff}}=1/2$ states and $J_{\text{eff}}=3/2$ states, respectively.

For $\Delta_{\text{tri}}^{\text{CF}} = 0$, t_{2g} - e_g splitting was fixed at 2.790 eV and all the off-diagonal matrix elements were zeroed in Eq. (1). The lowest six states in this case are represented by $\{\phi'_\alpha\}$, $\alpha = 1, 6$, while the lowest two states obtained using *true* CF from Eq. (1) are labeled as $\{\phi_\beta\}$, $\beta = 1-2$. The projections $\langle \phi'_\alpha | \phi_\beta \rangle$ are listed in Table I. From the table, since $|\langle \phi'_\alpha | \phi_\beta \rangle|^2 = 0.811$ for $\delta_{\alpha\beta} = 1, 2$, one can conclude that the $J_{\text{eff}}=1/2$ states retain their major weight despite a substantial $\Delta_{\text{tri}}^{\text{CF}}$, validating the applicability of the $J_{\text{eff}}=1/2$ picture in Sr₄RhO₆. The nonzero value of projections $|\langle \phi'_\alpha | \phi_\beta \rangle|^2$ ($\sim 0.026/0.010$) for $\alpha = 3-6$, $\beta = 1-2$ indicates a small admixture of the $J_{\text{eff}}=1/2$ and $3/2$ states due to $\Delta_{\text{tri}}^{\text{CF}}$. We find small changes of $\sim 4\%$ in these projections for $\lambda = 90$ meV.

One of the quantities which can be measured from the resonant inelastic x-ray scattering experiments is the single-point excitations represented by sharp peaks in the scattering intensity in the relevant energy range. It can be a direct probe for cubic symmetry lowering of the Rh-O₆ octahedra in

TABLE I. Projections of the $J_{\text{eff}}=1/2, 3/2$ states obtained when $\Delta_{\text{tri}}^{\text{CF}} = 0$, onto $J_{\text{eff}}=1/2$ states with *true* CF from Eq. (1). These states are obtained from exact diagonalization of the Hamiltonian in Eq. (2).

$\langle \phi'_\alpha $	$\langle \phi'_\alpha \phi_\beta \rangle$	
	$ \phi_1\rangle$	$ \phi_2\rangle$
1	0.901	0.352
2	0.352	0.901
3	0.162	0.056
4	0.056	0.162
5	0.101	0.117
6	0.117	0.101

Sr₄RhO₆. Theoretically, such low-lying crystal-field-assisted many-body excitations bear a close resemblance to the eigenvalues obtained from diagonalization of the many-body Hamiltonian in Eq. (2). For Sr₄RhO₆, analysis of the eigenvalue reveals that the $J_{\text{eff}}=3/2$ states split into two doublets by $E_2 = 0.133$ eV [see Fig. 1(a)], which would otherwise be fourfold degenerate if $\Delta_{\text{tri}}^{\text{CF}} = 0$. Energy separation of the $J_{\text{eff}}=1/2$ doublet with the lower $J_{\text{eff}}=3/2$ doublet is $E_1 = 0.181$ eV. It can also be observed that E_1 is ~ 30 meV smaller than the expected value of $\frac{3}{2}\lambda$ due to the finite $\Delta_{\text{tri}}^{\text{CF}}$. From the higher $J_{\text{eff}}=3/2$ doublets, the next single-ion excitation is at ~ 1.695 eV. From this point, a broad continuum of states with energy separations of few meV in the window of ~ 165 meV are found in our calculations. Having investigated the electronic properties of Sr₄RhO₆, we now discuss its magnetic properties in the next section.

C. Magnetism

We start by projecting the Hamiltonian in Eq. (2) to the pseudospins $J_{1/2}$ subspace and introduce hopping (H_{hop}) as a perturbation. The hopping amplitudes are extracted from H_{TB} and are listed in the Appendix Table III. In the limit $U \gg t$, the second-order perturbation term brings

$$\begin{aligned}
 H^{(2)} &= \sum_{ij} \sum_{\alpha\beta\alpha'\beta'} \mathcal{H}(i, j)_{\alpha\beta\alpha'\beta'} |i\alpha, j\beta\rangle \langle i\alpha', j\beta'|, \\
 \mathcal{H}(i, j)_{\alpha\beta\alpha'\beta'} &= \sum_{kl} \sum_{\gamma\lambda} \frac{1}{\Delta E} \langle i\alpha, j\beta | H_{\text{hop}} | k\gamma, l\lambda \rangle \\
 &\quad \times \langle k\gamma, l\lambda | H_{\text{hop}} | i\alpha', j\beta' \rangle, \quad (3)
 \end{aligned}$$

where $1/\Delta E = \frac{1}{2}[1/(E_{i\alpha} + E_{j\beta} - E_{k\lambda} - E_{l\gamma})]$. Here, $|i\alpha, j\beta\rangle$ and $|i\alpha', j\beta'\rangle$ are two-site states made of $J_{1/2}$ doublets, and $|k\lambda, l\gamma\rangle$ are two-site excited states with d^6 and d^4 configurations with Hilbert space dimensions of 210 for both. H_{hop} connects a two-site ground state to these excited states. The eigenstates of isolated Rh ions with four and six d electrons are obtained again by exact diagonalization.

One can represent the pseudospins $J_{1/2}$ as $S^\mu = \langle i\alpha | \mathbf{J}_{i, \text{eff}}^\mu | i\beta \rangle$, which are the expectation values of pseudospin $\mathbf{J}_{\text{eff}}^\mu$ operators with $\mu = 0, x, y, z$. Here, $\mathbf{J}_{\text{eff}}^0 = \mathbb{1}_{2 \times 2}$ is the matrix representation of operator $\mathbf{J}_{\text{eff}}^0$. Using it, Eq. (3) can

TABLE II. Estimated first-neighbor (NN) Heisenberg J , Kitaev K , and diagonal ζ and off-diagonal η , η' , η'' anisotropic terms on different bonds for Sr_4RhO_6 given in meV. The second-nearest-neighbor interactions were found to be negligibly small (<0.01 meV). Parameters used are $U = 2.474$ eV, $J_{\text{H}} = 0.106$ eV, and three values of $\lambda = 90, 140, 174$ meV.

Term	$\lambda = 90$ meV			$\lambda = 140$ meV			$\lambda = 174$ meV		
	A	B	C	A	B	C	A	B	C
J	0.149	-0.519	4.262	0.301	-0.109	3.250	0.402	-0.021	2.975
K	0.010	-1.737	0.473	0.015	-1.596	0.257	0.017	-1.544	0.193
ζ	-0.016	-0.488	-0.199	-0.017	-0.538	-0.125	-0.017	-0.555	-0.101
η	0.022	-2.246	1.066	0.017	-1.829	0.460	0.011	-1.686	0.296
η'	-0.016	1.040	-0.873	-0.014	0.683	-0.348	0.000	0.564	-0.207
η''	0.025	-1.231	0.723	0.019	-0.899	0.271	0.012	-0.784	0.154
D	0.000	-1.377	0.000	0.000	-0.666	0.000	0.000	-0.472	0.000
D'	0.000	2.518	0.000	0.000	1.608	0.000	0.000	1.332	0.000
D''	0.000	-2.303	0.000	0.000	-1.325	0.000	0.000	-1.041	0.000

be mapped to a spin Hamiltonian of the form

$$H_{\text{spin}} = S_i^\mu \Gamma(i, j)^{\mu\nu} S_j^\nu \\ = \Gamma(i, j)^{\mu\nu} \phi_{i\alpha}^\dagger S_{\alpha\alpha'}^\mu \phi_{i\alpha'} \phi_{j\beta} S_{\beta\beta'}^\nu \phi_{j\beta}^\dagger.$$

In the above expression, summation over all repeated indexes is implied. The map can be achieved by solving the linear equations,

$$-S_{\alpha\alpha'}^\mu S_{\beta\beta'}^\nu \Gamma(i, j)^{\mu\nu} = \mathcal{H}(i, j)_{\alpha\beta\alpha'\beta'}.$$

Here, degeneracy of the Kramers doublet leads to $\Gamma^{0\mu} = \Gamma^{\mu 0} = 0$. Thus, the most general form of the exchange interaction matrix on an Rh-Rh bond $l \in (i, j)$ is defined as

$$\Gamma_l = \begin{pmatrix} J + \zeta & \eta + D & \eta' - D' \\ \eta - D & J - \zeta & \eta'' + D'' \\ \eta' + D' & \eta'' - D'' & J + K \end{pmatrix}. \quad (4)$$

In the above expression, J , K , and η/η' are the Heisenberg, Kitaev, and off-diagonal interaction terms between the pseudospins-1/2, while ζ is the diagonal anisotropic term. The DMI is represented by the (D, D', D'') vector.

The Rh atoms form a body-centered cubic lattice in Sr_4RhO_6 and thus each Rh atom has eight 1NNs. Based on the nature of the magnetic interactions between different 1NNs, we subdivide the Rh-Rh bonds into three distinct categories, which are indicated as A/B/C/D bonds in Fig. 1(c). The values of the magnetic interactions are listed in Table II. For bonds A and C, the Γ_l matrix acquires a more symmetric form since on these bonds $\zeta = \eta = \eta' = \eta'' = D = D' = D'' = 0$. However, the magnetic interactions on these two bonds differ in their strengths. On the B bond, Γ_B takes the general form of Eq. (4) and Γ_D can be obtained by simply taking the transpose of Γ_B .

Several remarks are in order. First, one can see that the strength, as well as signs of interactions, differ for different bonds. For example, for the A and C bonds, J , η , and η' are antiferromagnetic, while for the B bond, they are ferromagnetic (FM), and the AFM Kitaev coupling is stronger on the B bond than the others. We emphasize that the AFM Kitaev coupling in Sr_4RhO_6 , although smaller, distinctly differs from the previous reports on iridates and $\alpha\text{-RuCl}_3$ [36,54]. Second,

quite interestingly, DMI appears on B and D bonds in the centrosymmetric structure of Sr_4RhO_6 . However, D , D' , and D'' have opposite signs on these two bonds. We attribute the appearance of DMI to the local inversion symmetry breaking due to the anisotropic crystalline potential produced by Sr atoms in the extended environment around Rh atoms, shown in Fig. 1(c). The hopping pathways for the first-nearest symmetry in equivalent Rh-Rh neighbors gets influenced by the crystalline potential produced by this extended environment, resulting in the $T_{ij}^t \neq T_{ij}$ form of hopping matrix in the Appendix Table III. The disappearance of DMI on the A and C bonds is merely an artifact of the local coordinate system that we choose for our H_{TB} . For DMI between two sites, it is always possible to make a local rotation of the spin coordinate axes at one of the sites to “gauge” away this interaction by rotating the coordinates around the axis of the DM vector by an angle corresponding to the classical canting angle [59]. We verified this point by choosing a set of different local axes in which DMI appears at both the A and C bonds, albeit smaller than the B and D bonds. Third, one may think that the Sr^{+2} ions on the A bond may mediate superexchange interaction between Rh atoms through their s orbitals. However, on the contrary, we find highly suppressed interactions on this bond, suggesting a destructive role of the anisotropic crystalline potential of the Sr^{+2} on magnetic interactions. Fourth, we found large off-diagonal terms on some of the Rh-Rh bonds. This is similar to the case of iridates and $\alpha\text{-RuCl}_3$ [54] resulting from substantial $\Delta_{\text{tri}}^{\text{CF}}$ distortions present in all these materials. Based on the two particularly noticeable features in the first two points, viz-a-viz AFM Kitaev terms and the appearance of DMI, one may consider Sr_4RhO_6 to be a distinct $4d$ magnetic material.

Varying the magnitude of SOC strength λ in our model does not change the interactions at a qualitative level. The estimated magnetic interactions for $\lambda = 90, 195$ meV are listed in Table II along with values for $\lambda = 140$ meV. The trend here is that with an increase of λ , the absolute values of all the magnetic interactions decrease, except the AFM J term on the A bond.

The magnetic interactions of Table II are used to optimize the classical magnetic state using the SPINW package [60]. The obtained magnetic ground state, represented by ordering

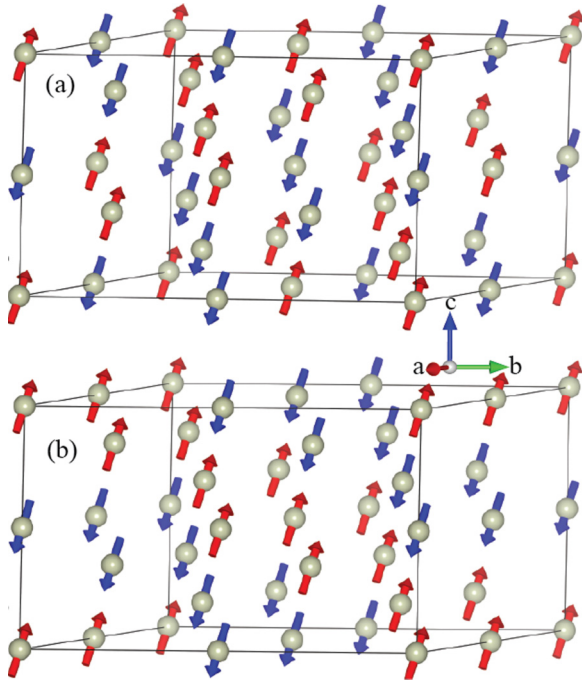


FIG. 4. (a) Experimentally proposed magnetic ground state of Sr₄RhO₆. (b) Classical ground state obtained after optimization using the exchange interactions of Table II. Color-coded spin orientation of only the Rh lattice is shown here.

vector $\sim(1.0 \ 0.5 \ 0)$, is shown in Fig. 4(b), along with the experimentally proposed one in Fig. 4(a). The AFM state obtained in our calculations successfully captures most of the experimental features. In the experimental magnetic structure, the spin arrangement on the Rh-Rh bonds [Fig. 1(c)] A and B is AFM, while on C and D it is FM. The optimized magnetic state in Fig. 4(b) from our calculations retains AFM coupling on A and FM coupling at D bonds. However, this configuration differs from the one shown in Fig. 4(a) on bonds B and C, where the spin arrangement in the two cases is just opposite to each other, i.e., on the B bond, the coupling is FM, while on the C bond, it is AFM in our optimized structure. Swapping the interactions at bonds B and C does not bring the experimentally observed ground state, indicating a joint meticulous effort of all the magnetic interactions to bring the ground state. We find a slight deviation of magnetic moments from the ac plane mainly due to the presence of off-diagonal terms such as $\eta/\eta'/\eta''$ and DMI. This is consistent with the experimental finding of small tilting from the c axis [46]. Our optimized magnetic configuration is energetically close to the experimentally proposed one, with the former stabilized by 1.552 meV/spin. The second- and third-neighbor magnetic interactions are found to be negligibly small in Sr₄RhO₆ and do not bring any distinguishable change in the optimization of the magnetic ground state. Thus we ignore them in further calculations of spin-wave spectra.

Here, we would like to comment that the scale of the magnetic ordering temperature of a material depends on various parameters such as the strength of exchange interactions, number of neighbors, their corresponding exchange contributions, and spatial dimensions of the magnetic lattice. Although

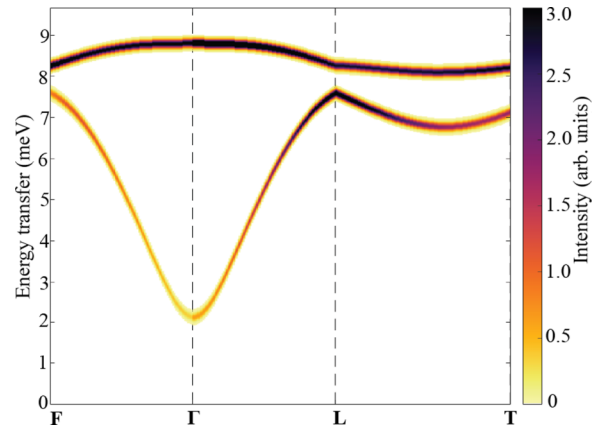


FIG. 5. Spin-wave spectrum of Sr₄RhO₆ obtained within linear spin-wave theory considering the magnetic interactions of Table II.

the magnetic lattice of the Rh atoms in Sr₄RhO₆ forms a three-dimensional bulk structure with eight first magnetic neighbors, the strongly frustrated anisotropic nature of bond-dependent magnetic interactions might be the reason behind its experimentally observed low T_N of ~ 7.5 K. We used the classical Monte Carlo technique implemented in the SPINW package [60] to estimate T_N for Sr₄RhO₆. The estimated value $T_N = 10.5$ K for interactions corresponding to $\lambda = 140$ meV in Table II is in close agreement with the experimental observation.

D. Spin-wave spectra

We further use the magnetic interactions listed in Table II in linear spin-wave theory to obtain the spin-wave spectra using the SPINW package [60]. The obtained spectrum along various reciprocal space directions are shown in Fig. 5.

Several points are to be noted about the spectrum. First, one can see that the spectrum is gapped along all directions in the reciprocal space with a Goldstone gap of ~ 2 meV. This feature of spin-wave spectrum may be caused by the breakdown of SU(2) symmetry of the isotropic Heisenberg Hamiltonian. Such a symmetry breaking can be a result of additional Ising-like Kitaev terms and/or diagonal/off-diagonal anisotropic terms such as ζ , η , η' , and η'' . Second, one branch ~ 8 meV in the spectrum appears to be dispersionless. It is separated from the dispersing branch by ~ 0.5 meV. Such a feature has previously been observed from the inelastic neutron scattering experiments on some of the cobaltates [16], which are pertinent material candidates for Kitaev physics [23]. Third, it can observe that the spin-wave spectrum near the Γ point are quadratic in nature. This is in contradiction to the expected linear dispersion of spin-wave dispersion for an AFM ground state.

In order to investigate the origin of the previously mentioned features of spin-wave spectrum of Sr₄RhO₆, we break it down to the contribution of either individual or a specific combination of magnetic interactions, and the plots are shown in Fig. 6. Such an analysis can provide useful insights as has been shown in Ntallis *et al.* [61] for the case of NaOsO₃.

Considering the J and K terms together, we immediately obtain both branches with a lower branch, at Γ , showing the

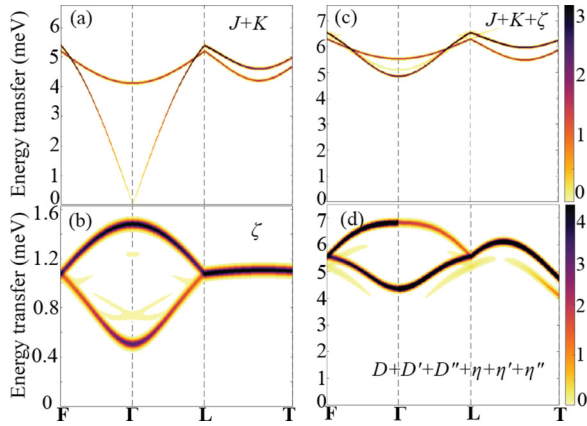


FIG. 6. Breakdown of spin-wave spectrum shown in Fig. 3 to individual contributions of a combination of various magnetic interactions. Spectra from (a) $J+K$ terms, (b) only diagonal anisotropic term ζ , (c) $J+K+\zeta$ terms, and (d) $D+D'+D''+\eta+\eta'+\eta''$ terms from Table II.

linear dispersion behavior of an antiferromagnet. The plot is shown in Fig. 6(a). However, the spectrum is barely gapped in this case due to dominant J over K which is also responsible for the dispersion width of ~ 5.5 meV of the lower branch. Consideration of the K -only term in the Hamiltonian produces a completely flat branch at ~ 4 meV (not shown), consistent with the previous theoretical study of the Kitaev model [62]. The ζ -only term indeed causes the gap opening along with a deviation towards a quadratic dispersion at Γ of the lower branch, as shown in Fig. 6(b). However, the energy scale, in this case, is smaller than that of the original spectrum in Fig. 5. A combination of $J+K+\zeta$ [Fig. 6(c)] reproduces some of the features in the more or less similar spectral windows as that of the original spectrum. However, the dispersion width and nature of the lower branch, in this case, are inconsistent with the original one in Fig. 5. Additionally, near Γ , dispersion of the lower branch appears to be further deviating from quadratic to higher powers of k . The terms $D+D'+D''+\eta+\eta'+\eta''$ produce similar but relatively flatter branches than the ζ terms, shown Fig. 6(d). The spectral energy window, in this case, is similar to that of the $J+K+\zeta$ term. Thus, one can say conclusively that the dominant off-diagonal terms are mainly responsible for the gap in the spin-wave spectrum of Sr_4RhO_6 , while the diagonal anisotropic term decides the nature of dispersion near the Γ point in the spin-wave spectrum of Sr_4RhO_6 . We would like to emphasize that our spin Hamiltonian does not contain the on-site anisotropic term shown to be responsible for opening the gap in the spin-wave spectrum of NaOsO_3 [61]. The overall spectrum of Sr_4RhO_6 , which resembles a typical magnetic

system with strong frustration, is a joint effort of all the terms of the magnetic Hamiltonian.

IV. CONCLUSION

In the quest for new Kitaev candidates, in this work, we have investigated the electronic and magnetic properties of Sr_4RhO_6 . Through *ab initio* calculations and a TB model, we show the lowering of cubic symmetry of RhO_6 octahedra due to additional trigonal-like distortions, which are in contradiction to the previous experimental proposal. Using the exact-diagonalization technique, we show that despite such a distortion, the electronic and magnetic properties of Sr_4RhO_6 can be well described with the pseudospin-1/2 framework. The magnetic interactions between these pseudospins were found to be highly bond-dependent anisotropic in nature. We found two particularly noticeable features of the 1NN magnetic interactions in Sr_4RhO_6 which are the appearance of the AFM Kitaev term and DMI. This may place Sr_4RhO_6 in a distinct class of materials as previously proposed Kitaev candidates shown to have FM Kitaev couplings and DMI that appears on the second-neighbor bonds [54]. The analysis of spin-wave spectrum obtained using linear spin-wave theory considering these interactions reveals the crucial role of diagonal and off-diagonal magnetic interactions in producing a gapped spectrum of Sr_4RhO_6 . Our theoretical study provides deeper insights about the coupling among the structural, electronic, and magnetic degrees of freedom in these compounds and calls for further experimental investigations.

ACKNOWLEDGMENTS

We have greatly benefited from stimulating discussions with Dr. Stephen M. Winter and gratefully acknowledge his critical reading of our manuscript and valuable feedback. We acknowledge financial supports from the National Natural Science Foundation of China (Grants No. 12274003, No. 11725415 and No. 11934001), the National Key R&D Program of China (Grants No. 2018YFA0305601 and No. 2021YFA1400100), and the Innovation Program for Quantum Science and Technology (Grant No. 2021ZD0302600). This work is also partially supported by the China Postdoctoral Science Foundation (Grant No. 2022M710231) awarded to Q.G.

APPENDIX: FIRST-NEIGHBOR Rh-Rh HOPPING AMPLITUDES IN Sr_4RhO_6 EXPRESSED IN THE BASIS

$$(d_{z^2}^\dagger, d_{x^2-y^2}^\dagger, d_{xz}^\dagger, d_{yz}^\dagger, d_{xy}^\dagger)$$

TABLE III. First-neighbor Rh-Rh hopping amplitudes on the different types of bonds shown in Fig. 1(c).

A bond	B bond	C bond
$\begin{pmatrix} -0.0251 & -0.0042 & -0.0015 & 0.0144 & 0.0217 \\ -0.0042 & 0.0270 & 0.0182 & 0.0131 & -0.0094 \\ -0.0015 & 0.0182 & -0.0288 & 0.0240 & -0.0319 \\ 0.0144 & 0.0131 & 0.0240 & -0.0369 & 0.0263 \\ 0.0217 & -0.0094 & -0.0319 & 0.0263 & -0.0199 \end{pmatrix}$	$\begin{pmatrix} 0.0245 & 0.0006 & -0.0302 & 0.0517 & 0.0141 \\ 0.0368 & -0.0040 & -0.0626 & 0.0285 & 0.0339 \\ -0.0334 & -0.0077 & -0.0100 & 0.0009 & -0.0192 \\ -0.0791 & -0.0004 & 0.0633 & 0.0175 & 0.0087 \\ 0.0476 & -0.0294 & 0.0256 & 0.0130 & 0.0033 \end{pmatrix}$	$\begin{pmatrix} -0.0083 & 0.0134 & -0.0001 & -0.0217 & -0.0419 \\ 0.0134 & -0.0245 & 0.0618 & 0.0233 & 0.0622 \\ -0.0001 & 0.0618 & -0.0173 & -0.0057 & 0.0128 \\ -0.0217 & 0.0233 & -0.0057 & -0.0194 & 0.0103 \\ -0.0419 & 0.0622 & 0.0128 & 0.0103 & -0.0684 \end{pmatrix}$

- [1] M. Z. Hasan and C. L. Kane, Colloquium: Topological insulators, *Rev. Mod. Phys.* **82**, 3045 (2010).
- [2] M. Z. Hasan and J. E. Moore, Three-dimensional topological insulators, *Annu. Rev. Condens. Matter Phys.* **2**, 55 (2011).
- [3] X.-L. Qi and S.-C. Zhang, Topological insulators and superconductors, *Rev. Mod. Phys.* **83**, 1057 (2011).
- [4] W. Witczak-Krempa, G. Chen, Y. B. Kim, and L. Balents, Correlated quantum phenomena in the strong spin-orbit regime, *Annu. Rev. Condens. Matter Phys.* **5**, 57 (2014).
- [5] J. G. Rau, E. K.-H. Lee, and H.-Y. Kee, Spin-orbit physics giving rise to novel phases in correlated systems: Iridates and related materials, *Annu. Rev. Condens. Matter Phys.* **7**, 195 (2016).
- [6] P. Anderson, Resonating valence bonds: A new kind of insulator?, *Mater. Res. Bull.* **8**, 153 (1973).
- [7] J. Kim, D. Casa, M. H. Upton, T. Gog, Y.-J. Kim, J. F. Mitchell, M. van Veenendaal, M. Daghofer, J. van den Brink, G. Khaliullin, and B. J. Kim, Magnetic Excitation Spectra of Sr_2IrO_4 Probed by Resonant Inelastic X-Ray Scattering: Establishing Links to Cuprate Superconductors, *Phys. Rev. Lett.* **108**, 177003 (2012).
- [8] G. Khaliullin, W. Koshibae, and S. Maekawa, Low Energy Electronic States and Triplet Pairing in Layered Cobaltate, *Phys. Rev. Lett.* **93**, 176401 (2004).
- [9] H. Y. Hwang, Y. Iwasa, M. Kawasaki, B. Keimer, N. Nagaosa, and Y. Tokura, Emergent phenomena at oxide interfaces, *Nat. Mater.* **11**, 103 (2012).
- [10] G. Jackeli and G. Khaliullin, Mott Insulators in the Strong Spin-Orbit Coupling Limit: From Heisenberg to a Quantum Compass and Kitaev Models, *Phys. Rev. Lett.* **102**, 017205 (2009).
- [11] A. Kitaev, Anyons in an exactly solved model and beyond, *Ann. Phys.* **321**, 2 (2006), January Special Issue.
- [12] L. Clark and A. H. Abdeldaim, Quantum spin liquids from a materials perspective, *Annu. Rev. Mater. Res.* **51**, 495 (2021).
- [13] H. Takagi, T. Takayama, G. Jackeli, G. Khaliullin, and S. E. Nagler, Concept and realization of Kitaev quantum spin liquids, *Nat. Rev. Phys.* **1**, 264 (2019).
- [14] H. Liu and G. Khaliullin, Pseudospin exchange interactions in d^7 cobalt compounds: Possible realization of the Kitaev model, *Phys. Rev. B* **97**, 014407 (2018).
- [15] R. Sano, Y. Kato, and Y. Motome, Kitaev-Heisenberg Hamiltonian for high-spin d^7 Mott insulators, *Phys. Rev. B* **97**, 014408 (2018).
- [16] M. Songvilay, J. Robert, S. Petit, J. A. Rodriguez-Rivera, W. D. Ratcliff, F. Damay, V. Balédent, M. Jiménez-Ruiz, P. Lejay, E. Pachoud, A. Hadj-Azzem, V. Simonet, and C. Stock, Kitaev interactions in the Co honeycomb antiferromagnets $\text{Na}_3\text{Co}_2\text{SbO}_6$ and $\text{Na}_2\text{Co}_2\text{TeO}_6$, *Phys. Rev. B* **102**, 224429 (2020).
- [17] H. Liu, J. c. v. Chaloupka, and G. Khaliullin, Kitaev Spin Liquid in $3d$ Transition Metal Compounds, *Phys. Rev. Lett.* **125**, 047201 (2020).
- [18] L. Viciu, Q. Huang, E. Morosan, H. Zandbergen, N. Greenbaum, T. McQueen, and R. Cava, Structure and basic magnetic properties of the honeycomb lattice compounds $\text{Na}_2\text{Co}_2\text{TeO}_6$ and $\text{Na}_3\text{Co}_2\text{SbO}_6$, *J. Solid State Chem.* **180**, 1060 (2007).
- [19] G. Xiao, Z. Xia, W. Zhang, X. Yue, S. Huang, X. Zhang, F. Yang, Y. Song, M. Wei, H. Deng, and D. Jiang, Crystal growth and the magnetic properties of $\text{Na}_2\text{Co}_2\text{TeO}_6$ with quasi-two-dimensional honeycomb lattice, *Cryst. Growth Des.* **19**, 2658 (2019).
- [20] E. Lefrançois, M. Songvilay, J. Robert, G. Nataf, E. Jordan, L. Chaix, C. V. Colin, P. Lejay, A. Hadj-Azzem, R. Ballou, and V. Simonet, Magnetic properties of the honeycomb oxide $\text{Na}_2\text{Co}_2\text{TeO}_6$, *Phys. Rev. B* **94**, 214416 (2016).
- [21] A. K. Bera, S. M. Yusuf, A. Kumar, and C. Ritter, Zigzag antiferromagnetic ground state with anisotropic correlation lengths in the quasi-two-dimensional honeycomb lattice compound $\text{Na}_2\text{Co}_2\text{TeO}_6$, *Phys. Rev. B* **95**, 094424 (2017).
- [22] W. Chen, X. Li, Z. Hu, Z. Hu, L. Yue, R. Sutarto, F. He, K. Iida, K. Kamazawa, W. Yu, X. Lin, and Y. Li, Spin-orbit phase behavior of $\text{Na}_2\text{Co}_2\text{TeO}_6$ at low temperatures, *Phys. Rev. B* **103**, L180404 (2021).
- [23] S. K. Pandey and J. Feng, Spin interaction and magnetism in cobaltate Kitaev candidate materials: An *ab initio* and model Hamiltonian approach, *Phys. Rev. B* **106**, 174411 (2022).
- [24] J. Chaloupka, G. Jackeli, and G. Khaliullin, Kitaev-Heisenberg Model on a Honeycomb Lattice: Possible Exotic Phases in Iridium Oxides A_2IrO_3 , *Phys. Rev. Lett.* **105**, 027204 (2010).
- [25] Y. Singh, S. Manni, J. Reuther, T. Berlijn, R. Thomale, W. Ku, S. Trebst, and P. Gegenwart, Relevance of the Heisenberg-Kitaev Model for the Honeycomb Lattice Iridates A_2IrO_3 , *Phys. Rev. Lett.* **108**, 127203 (2012).
- [26] Y. Singh and P. Gegenwart, Antiferromagnetic Mott insulating state in single crystals of the honeycomb lattice material Na_2IrO_3 , *Phys. Rev. B* **82**, 064412 (2010).
- [27] S. K. Choi, R. Coldea, A. N. Kolmogorov, T. Lancaster, I. I. Mazin, S. J. Blundell, P. G. Radaelli, Y. Singh, P. Gegenwart, K. R. Choi, S.-W. Cheong, P. J. Baker, C. Stock, and J. Taylor, Spin Waves and Revised Crystal Structure of Honeycomb Iridate Na_2IrO_3 , *Phys. Rev. Lett.* **108**, 127204 (2012).
- [28] A. Biffin, R. D. Johnson, S. Choi, F. Freund, S. Manni, A. Bombardi, P. Manuel, P. Gegenwart, and R. Coldea, Unconventional magnetic order on the hyperhoneycomb Kitaev lattice in $\beta\text{-Li}_2\text{IrO}_3$: Full solution via magnetic resonant x-ray diffraction, *Phys. Rev. B* **90**, 205116 (2014).
- [29] A. Biffin, R. D. Johnson, I. Kimchi, R. Morris, A. Bombardi, J. G. Analytis, A. Vishwanath, and R. Coldea, Noncoplanar and Counterrotating Incommensurate Magnetic Order Stabilized by Kitaev Interactions in $\gamma\text{-Li}_2\text{IrO}_3$, *Phys. Rev. Lett.* **113**, 197201 (2014).
- [30] B. H. Kim, G. Khaliullin, and B. I. Min, Electronic excitations in the edge-shared relativistic Mott insulator: Na_2IrO_3 , *Phys. Rev. B* **89**, 081109(R) (2014).
- [31] H. Gretarsson, J. P. Clancy, X. Liu, J. P. Hill, E. Bozin, Y. Singh, S. Manni, P. Gegenwart, J. Kim, A. H. Said, D. Casa, T. Gog, M. H. Upton, H.-S. Kim, J. Yu, V. M. Katukuri, L. Hozoi, J. van den Brink, and Y.-J. Kim, Crystal-Field Splitting and Correlation Effect on the Electronic Structure of A_2IrO_3 , *Phys. Rev. Lett.* **110**, 076402 (2013).
- [32] K. W. Plumb, J. P. Clancy, L. J. Sandilands, V. V. Shankar, Y. F. Hu, K. S. Burch, H.-Y. Kee, and Y.-J. Kim, $\alpha\text{-RuCl}_3$: A spin-orbit assisted Mott insulator on a honeycomb lattice, *Phys. Rev. B* **90**, 041112(R) (2014).
- [33] R. D. Johnson, S. C. Williams, A. A. Haghighirad, J. Singleton, V. Zapf, P. Manuel, I. I. Mazin, Y. Li, H. O. Jeschke, R. Valentí, and R. Coldea, Monoclinic crystal structure of $\alpha\text{-RuCl}_3$ and the zigzag antiferromagnetic ground state, *Phys. Rev. B* **92**, 235119 (2015).

- [34] A. Banerjee, C. A. Bridges, J.-Q. Yan, A. A. Aczel, L. Li, M. B. Stone, G. E. Granroth, M. D. Lumsden, Y. Yiu, J. Knolle, S. Bhattacharjee, D. L. Kovrizhin, R. Moessner, D. A. Tennant, D. G. Mandrus, and S. E. Nagler, Proximate Kitaev quantum spin liquid behaviour in a honeycomb magnet, *Nat. Mater.* **15**, 733 (2016).
- [35] H.-S. Kim, V. S. V., A. Catuneanu, and H.-Y. Kee, Kitaev magnetism in honeycomb RuCl_3 with intermediate spin-orbit coupling, *Phys. Rev. B* **91**, 241110(R) (2015).
- [36] W. Wang, Z.-Y. Dong, S.-L. Yu, and J.-X. Li, Theoretical investigation of magnetic dynamics in $\alpha - \text{RuCl}_3$, *Phys. Rev. B* **96**, 115103 (2017).
- [37] A. M. Cook, S. Matern, C. Hickey, A. A. Aczel, and A. Paramakanti, Spin-orbit coupled $j_{\text{eff}} = 1/2$ iridium moments on the geometrically frustrated fcc lattice, *Phys. Rev. B* **92**, 020417(R) (2015).
- [38] G. Cao, A. Subedi, S. Calder, J.-Q. Yan, J. Yi, Z. Gai, L. Poudel, D. J. Singh, M. D. Lumsden, A. D. Christianson, B. C. Sales, and D. Mandrus, Magnetism and electronic structure of $\text{La}_2\text{ZnIrO}_6$ and $\text{La}_2\text{MgIrO}_6$: Candidate $J_{\text{eff}} = \frac{1}{2}$ Mott insulators, *Phys. Rev. B* **87**, 155136 (2013).
- [39] A. A. Aczel, A. M. Cook, T. J. Williams, S. Calder, A. D. Christianson, G.-X. Cao, D. Mandrus, Y.-B. Kim, and A. Paramakanti, Highly anisotropic exchange interactions of $j_{\text{eff}} = \frac{1}{2}$ iridium moments on the fcc lattice in La_2bIrO_6 ($b = \text{Mg}, \text{Zn}$), *Phys. Rev. B* **93**, 214426 (2016).
- [40] S. Kanungo, K. Mogare, B. Yan, M. Reehuis, A. Hoser, C. Felser, and M. Jansen, Weak orbital ordering of Ir t_{2g} states in the double perovskite $\text{Sr}_2\text{CeIrO}_6$, *Phys. Rev. B* **93**, 245148 (2016).
- [41] W. K. Zhu, C.-K. Lu, W. Tong, J. M. Wang, H. D. Zhou, and S. X. Zhang, Strong ferromagnetism induced by canted antiferromagnetic order in double perovskite iridates $(\text{La}_{1-x}\text{Sr}_x)_2\text{ZnIrO}_6$, *Phys. Rev. B* **91**, 144408 (2015).
- [42] Y. Luo, C. Cao, B. Si, Y. Li, J. Bao, H. Guo, X. Yang, C. Shen, C. Feng, J. Dai, G. Cao, and Z.-a. Xu, Li_2RhO_3 : A spin-glassy relativistic Mott insulator, *Phys. Rev. B* **87**, 161121(R) (2013).
- [43] V. M. Katukuri, K. Roszeitis, V. Yushankhai, A. Mitrushchenkov, H. Stoll, M. van Veenendaal, P. Fulde, J. van den Brink, and L. Hozoi, Electronic structure of low-dimensional $4d5$ oxides: Interplay of ligand distortions, overall lattice anisotropy, and spin-orbit interactions, *Inorg. Chem.* **53**, 4833 (2014).
- [44] T. Birol and K. Haule, $J_{\text{eff}} = 1/2$ Mott-Insulating State in Rh and Ir Fluorides, *Phys. Rev. Lett.* **114**, 096403 (2015).
- [45] J. F. Vente, J. K. Lear, and P. D. Battle, $\text{Sr}_4\text{CaRhO}_6$: A magnetically ordered Rh compound, *J. Mater. Chem.* **5**, 1785 (1995).
- [46] S. Calder, L. Li, S. Okamoto, Y. Choi, R. Mukherjee, D. Haskel, and D. Mandrus, Spin-orbit driven magnetic insulating state with $J_{\text{eff}} = \frac{1}{2}$ character in a $4d$ oxide, *Phys. Rev. B* **92**, 180413(R) (2015).
- [47] G. Kresse and D. Joubert, From ultrasoft pseudopotentials to the projector augmented-wave method, *Phys. Rev. B* **59**, 1758 (1999).
- [48] P. E. Blöchl, Projector augmented-wave method, *Phys. Rev. B* **50**, 17953 (1994).
- [49] G. Kresse and J. Furthmüller, Efficient iterative schemes for *ab initio* total-energy calculations using a plane-wave basis set, *Phys. Rev. B* **54**, 11169 (1996).
- [50] J. P. Perdew, K. Burke, and M. Ernzerhof, Generalized Gradient Approximation Made Simple, *Phys. Rev. Lett.* **77**, 3865 (1996).
- [51] A. I. Liechtenstein, V. I. Anisimov, and J. Zaanen, Density-functional theory and strong interactions: Orbital ordering in Mott-Hubbard insulators, *Phys. Rev. B* **52**, R5467 (1995).
- [52] A. A. Mostofi, J. R. Yates, Y.-S. Lee, I. Souza, D. Vanderbilt, and N. Marzari, WANNIER90: A tool for obtaining maximally-localised Wannier functions, *Comput. Phys. Commun.* **178**, 685 (2008).
- [53] Q. Gu, S. K. Pandey, and R. Tiwari, A computational method to estimate spin-orbital interaction strength in solid state systems, *Comput. Mater. Sci.* **221**, 112090 (2023).
- [54] S. M. Winter, Y. Li, H. O. Jeschke, and R. Valentí, Challenges in design of Kitaev materials: Magnetic interactions from competing energy scales, *Phys. Rev. B* **93**, 214431 (2016).
- [55] G. Jha and T. Heine, DFTB parameters for the periodic table: part III, spin-orbit coupling, *J. Chem. Theory Comput.* **18**, 4472 (2022).
- [56] S. L. Adler, Quantum theory of the dielectric constant in real solids, *Phys. Rev.* **126**, 413 (1962).
- [57] N. Wiser, Dielectric constant with local field effects included, *Phys. Rev.* **129**, 62 (1963).
- [58] F. Aryasetiawan, M. Imada, A. Georges, G. Kotliar, S. Biermann, and A. I. Liechtenstein, Frequency-dependent local interactions and low-energy effective models from electronic structure calculations, *Phys. Rev. B* **70**, 195104 (2004).
- [59] I. Affleck and M. Oshikawa, Field-induced gap in Cu benzoate and other $s = \frac{1}{2}$ antiferromagnetic chains, *Phys. Rev. B* **60**, 1038 (1999).
- [60] S. Toth and B. Lake, Linear spin wave theory for single- q incommensurate magnetic structures, *J. Phys.: Condens. Matter* **27**, 166002 (2015).
- [61] N. Ntallis, V. Borisov, Y. O. Kvashnin, D. Thonig, E. Sjöqvist, A. Bergman, A. Delin, O. Eriksson, and M. Pereiro, Connection between magnetic interactions and the spin-wave gap of the insulating phase of NaOsO_3 , *Phys. Rev. B* **104**, 134433 (2021).
- [62] J. Knolle, D. L. Kovrizhin, J. T. Chalker, and R. Moessner, Dynamics of a Two-Dimensional Quantum Spin Liquid: Signatures of Emergent Majorana Fermions and Fluxes, *Phys. Rev. Lett.* **112**, 207203 (2014).